Published OnlineFirst June 1, 2015; DOI: 10.1158/1078-0432.CCR-15-0013

Cancer Therapy: Preclinical

Clinical Cancer Research

Tumor-Targeted Synergistic Blockade of MAPK and PI3K from a Layer-by-Layer Nanoparticle

Erik C. Dreaden[1,2], Yi Wen Kong[1,3], Stephen W. Morton[1,2], Santiago Correa[1,4], Ki Young Choi[1,2], Kevin E. Shopsowitz[1,2], Kasper Renggli[1,2,4], Ronny Drapkin[5,6,7], Michael B. Yaffe[1,3,4,8], and Paula T. Hammond[1,2,9]

Abstract

Purpose: Cross-talk and feedback between the RAS/RAF/MEK/ERK and PI3K/AKT/mTOR cell signaling pathways is critical for tumor initiation, maintenance, and adaptive resistance to targeted therapy in a variety of solid tumors. Combined blockade of these pathways—horizontal blockade—is a promising therapeutic strategy; however, compounded dose-limiting toxicity of free small molecule inhibitor combinations is a significant barrier to its clinical application.

Experimental Design: AZD6244 (selumetinib), an allosteric inhibitor of Mek1/2, and PX-866, a covalent inhibitor of PI3K, were co-encapsulated in a tumor-targeting nanoscale drug formulation—layer-by-layer (LbL) nanoparticles. Structure, size, and surface charge of the nanoscale formulations were characterized, in addition to *in vitro* cell entry, synergistic cell killing, and combined signal blockade. *In vivo* tumor targeting and therapy was investigated in breast tumor xenograft–bearing NCR nude mice by live animal fluorescence/bioluminescence imaging, Western blotting, serum cytokine analysis, and immunohistochemistry.

Results: Combined MAPK and PI3K axis blockade from the nanoscale formulations (160 ± 20 nm, −40 ± 1 mV) was synergistically toxic toward triple-negative breast (MDA-MB-231) and RAS-mutant lung tumor cells (KP7B) *in vitro*, effects that were further enhanced upon encapsulation. *In vivo*, systemically administered LbL nanoparticles preferentially targeted subcutaneous MDA-MB-231 tumor xenografts, simultaneously blocked tumor-specific phosphorylation of the terminal kinases Erk and Akt, and elicited significant disease stabilization in the absence of dose-limiting hepatotoxic effects observed from the free drug combination. Mice receiving untargeted, but dual drug–loaded nanoparticles exhibited progressive disease.

Conclusions: Tumor-targeting nanoscale drug formulations could provide a more safe and effective means to synergistically block MAPK and PI3K in the clinic. *Clin Cancer Res; 21(19); 4410–9. ©2015 AACR.*

Introduction

Combination chemotherapy has been a mainstay of clinical oncology since the mid 1960s (1, 2). While initially proposed to exploit nonoverlapping toxicity profiles of cytotoxic chemotherapeutics, recent advances in cancer cell signaling and the discovery of potent and selective small-molecule inhibitors have led to the development of rational combination approaches to cancer chemotherapy. These strategies can prime cancer cells for apoptosis (3, 4), abrogate mechanisms for resistance (5–9), block cancer cell-cycle progression (10), or dynamically rewire DNA damage response pathways (11, 12)—all leading to enhanced tumor cell killing.

Although combination therapies can be curative in a subset of malignancies (13), inefficient delivery limits the safety and efficacy of cooperative drug combinations that require cellular colocalization for effective cell killing. This can be difficult to achieve with traditional pharmaceutical excipients as synergistic compounds often exhibit vastly different physiochemical properties (e.g., size, charge, lipophilicity, and stability) that necessitate separate drug carriers. Colocalized delivery of cooperative drug combinations from single, multicomponent delivery vehicles can improve both therapeutic index (5) and treatment outcomes (6, 9, 12, 14) compared with combinations of individual carriers; however, tissue-specific delivery remains a significant challenge.

[1]Koch Institute for Integrative Cancer Research, Massachusetts Institute of Technology, Cambridge, Massachusetts. [2]Department of Chemical Engineering, Massachusetts Institute of Technology, Cambridge, Massachusetts. [3]Department of Biology, Massachusetts Institute of Technology, Cambridge, Massachusetts. [4]Department of Biological Engineering, Massachusetts Institute of Technology, Cambridge, Massachusetts. [5]Penn Ovarian Cancer Research Center, Basser Research Center for BRCA, University of Pennsylvania, Philadelphia, Pennsylvania. [6]Perelman Center for Advanced Medicine, Abramson Cancer Center, University of Pennsylvania, Philadelphia, Pennsylvania. [7]Department of Obstetrics and Gynecology, University of Pennsylvania, Philadelphia, Pennsylvania. [8]Division of Acute Care Surgery, Trauma, and Critical Care, Department of Surgery, Beth Israel Deaconess Medical Center, Harvard Medical School, Boston, Massachusetts. [9]Institute for Soldier Nanotechnologies, Massachusetts Institute of Technology, Cambridge, Massachusetts.

Note: Supplementary data for this article are available at Clinical Cancer Research Online (http://clincancerres.aacrjournals.org/).

Corresponding Authors: Paula T. Hammond, Massachusetts Institute of Technology, 77 Massachusetts Avenue, Cambridge, MA 02139. Phone: 1-617-2587577; Fax: 1-617-2588992; E-mail: hammond@mit.edu; and Michael B. Yaffe, Massachusetts Institute of Technology, Broad Institute, Beth Israel Deaconess Medical Center and Harvard Medical School, 77 Massachusetts Avenue, Cambridge, MA 02139. Phone: 1-617-4522442; E-mail: myaffe@mit.edu

doi: 10.1158/1078-0432.CCR-15-0013

Published OnlineFirst June 1, 2015; DOI: 10.1158/1078-0432.CCR-15-0013

Translational Relevance

The MAPK and PI3K cell signaling pathways encompass numerous clinically approved drug targets, and recent evidence suggests that cross-talk/feedback between these pathways is critical for initiation and maintenance of various solid tumors, as well as resistance to targeted therapies. Simultaneous blockade of these two signaling axes is a promising therapeutic strategy; however, rational combinations approaches with small-molecule inhibitors are poorly tolerated in patients. In this work, we develop a tumor-targeting nanoscale drug formulation based on layer-by-layer (LbL) self-assembly that horizontally blocks MAPK and PI3K signaling *in vitro* and *in vivo*, selectively inhibiting disease progression in tumor-bearing mice. These self-assembled drug carriers co-delivered synergistic drug compounds with vastly differing physiochemical properties, in a manner that pre-empted adaptive resistance and diminished toxic effects of the free drug combination. This approach could provide a more safe and effective means to synergistically block MAPK and PI3K in the clinic.

Nanoscale drug carriers that deliver cooperative drug combinations in a tumor-targeted fashion are urgently needed in the clinic.

Layer-by-layer (LbL) nanoparticles (15–24) are a new class of self-assembled polymer drug carriers that addresses challenges in the delivery of combination therapeutics. These structures consist of a functional nanoparticle core, a polyelectrolyte multilayer shell, and an exterior tumor-targeting stealth layer. Previously, we developed an LbL nanoparticle architecture that targets solid tumors through 3 independent mechanisms: (i) size-dependent passive tumor targeting, (ii) active, ligand-directed targeting of cell surface CD44 receptor, and (iii) hypoxic tumor pH-responsive cellular delivery (24). Here, we apply multimodal tumor-targeting LbL nanoparticles to drug solid tumors with a synergistic combination of small-molecule inhibitors that block known resistance pathways to MAPK and PI3K axis therapies.

The MAPK (RAS/RAF/MEK/ERK; ref. 25) and PI3K/AKT/mTOR (26) pathways are among the most frequently deregulated cell signaling pathways in human cancer. Activating mutations in *RAS* and *BRAF* are observed in 20% to 30% and 8% of human tumors, respectively (27–29), with *PTEN* and *PIK3CA* mutations occurring in 30% to 50% and 4% to 32%, respectively (30, 31). Aberrant activation of either pathway is capable of transforming cells *in vivo* in the appropriate genetic mutant background (32, 33), and the co-existence of mutations along both pathways is approximately twice as prevalent among advanced solid tumors (34). Although various proteins or upstream effectors of these signal cascades are clinically druggable (e.g., receptor tyrosine kinases, BRAF, MEK, PI3K, Akt, and mTOR), durable responses to molecularly targeted therapies has been difficult to achieve, due in part to extensive cross-talk and compensatory feedback between MAPK and PI3K signaling pathways (35). Upregulated MAPK signaling, for example, has been implicated in adaptive resistance to PI3K (36), Akt (37), and mTOR (38) inhibitors. Conversely, augmented PI3K signaling has been shown to contribute to resistance toward EGFR (39), BRAF (40), and MEK (41) inhibitors. PI3K signaling is also known to predicate maintenance of RAS-dependent lung tumors (33, 42), and cross-talk between these 2 pathways is known to be required for RAS-dependent angiogenesis (43).

Horizontal blockade of MAPK and PI3K has been proposed as a means to achieve synergistic cell killing and to abrogate adaptive resistance to single-axis targeted therapies. Engelman and colleagues found that combined MEK and PI3K/mTOR inhibition was synergistic against genetically engineered mouse models of KRAS-mutant non–small cell lung cancer (33). Similarly, Posch and colleagues reported that that dual inhibition of MEK and PI3K/mTOR was both synergistic and required for durable treatment response in NRAS-mutant melanoma *in vitro* and *in vivo* (44). A recent phase I clinical trial investigating simultaneous (i.e., horizontal) blockade of MAPK and PI3K in patients with refractory solid tumors found that dual inhibition may exhibit favorable efficacy compared with single-axis therapy, albeit with compounded and often dose-limiting toxicity (45). Here, we address this unmet clinical need by engineering nanoscale drug carriers that improve the therapeutic index of this novel combination therapy through multimodal targeted delivery to solid tumors. These modular, dual drug–containing delivery vehicles horizontally block MAPK and PI3K signaling to diminish tumor growth *in vivo*. Nanotechnology-enabled horizontal blockade of MAPK and PI3K is a promising strategy for the treatment of several solid tumor types and is demonstrated here in triple-negative breast cancer tumor models.

Materials and Methods

Materials

Poly(L-lysine) HBr (PLL, 15–30 kDa; Sigma-Aldrich), hyaluronan (HA, 200 kDa; Lifecore), and dextran sulfate sodium salt (DXS, 20 kDa; Sigma-Aldrich) were used as-received without further modification. Antibodies included total Akt (CST 4691), cleaved caspase-3 (CST 9661), total Erk (CST 4370), pAkt (CST 4060; S473), pAkt-Alexa Fluor 488 (Millipore CS203310; S473), pErk1/2 (CST 4370; T202/204, T185/187), and pErk1/2-PE (Millipore CS203329; T202/204, T185/187).

Nanoparticle synthesis and characterization

LbL nanoparticle assembly was performed as described previously (24). Liposomes were prepared by the sonication/extrusion method. Briefly, a chloroform mixture of DOTAP/DOPE/cholesterol (35:35:30 mol ratio, Avanti) was dried under nitrogen and stored overnight under vacuum. The lipid film was hydrated with a PBS solution of AZD6244 (Selleck) and PX-866 (LC Laboratories) at 18 wt%, each and immersed in a bath sonicator (55 °C) for 1 hour. The crude liposomes were extruded through a 50-nm polycarbonate membrane syringe extruder (Avanti) at 55°C, dialyzed against PBS for 48 hours (3.5-5 MWCO), and stored at 4°C for <1 week before use. Drug loading was quantified by HPLC (Agilent Technologies) in 50:50 acetonitrile/water (pH 5). Cryogenic transmission electron microscopy (TEM) was performed using a JEOL 2100 FEG instrument. Photon correlation spectroscopy and laser Doppler electrophoresis measurements were carried out using a Malvern Zetasizer Nano ZS90 particle analyser (λ = 633 nm, material/dispersant RI 1.590/1.330). Chemical properties were computed using ACD/Labs software (pH 7.4).

Cell culture

OVCAR-3, Hep G2, and MDA-MB-231 cells were obtained from ATCC. Murine KP7B cells were a gift from the laboratory of Tyler Jacks (46); these cells were obtained from the murine KP model of lung adenocarcinoma ($Kras^{LSL\text{-}G12D/wt}$;$p53^{flox/flox}$) that

Published OnlineFirst June 1, 2015; DOI: 10.1158/1078-0432.CCR-15-0013

exhibits conditional activation of oncogenic Ras. Cells were subcultured in DMEM supplanted with 10% FBS and penicillin/streptomycin or the supplier's recommended basal medium in a 5% CO_2 humidified atmosphere.

In vitro experiments

Viability was assessed by CellTiter-Glo assay (Promega) and normalized to vehicle controls. The Bliss expectation was calculated as $(A + B) - (A \times B)$, in which A and B are the fractional growth inhibitions induced by agents A and B at a given dose, respectively (47). Signaling was assessed in MDA-MB-231 cells serum-starved for 24 hours and then treated with drugs and/or particles and serum-stimulated (10% v/v FBS) for the times indicated. Cells were analyzed by flow cytometry or scraped, pelleted, and lysed in RIPA buffer containing protease/phosphatase inhibitor for Western blotting. Densitometry was calculated using ImageJ software. Statistical significance was assessed by the unpaired Student *t* test.

Fluorescence imaging

Hep G2 tumor spheroids (low CD44 expression) were prepared as described previously (24) and incubated for 3 hours in PBS containing 0.17 nmol/L LbL nanoparticles. Tumor spheroids were fixed in 3.7% paraformaldehyde for 30 minutes at room temperature, permeabilized with 0.1% Triton X-100 (PBS) for 5 minutes at room temperature, stained with Alexa Fluor 568 phalloidin (Life Technologies) for 30 minutes at room temperature, and inverted/mounted with Fluoromount onto 35-mm MatTek dishes. Fluorescent carboxylate-modified polystyrene beads (100 nm; Sigma-Aldrich; Orange 481/644) were substituted for dextran sulfate–layered liposomes to facilitate visualization of cellular localization. Slides were mounted and imaged using a Nikon 1AR Ultra-Fast Spectral Scanning Confocal Microscope.

Flow cytometry

Endocytotic inhibition was assessed using a BD LSR II flow cytometer following 1-hour preincubation in complete growth media supplanted with 10 mmol/L sodium azide/50 mmol/L 2-deoxy-D-glycose (ATP inhibition), 200 μmol/L genistein (caveolin inhibition), 10 μmol/L chlorpromazine (clathrin inhibition), 10 μmol/L wortmannin (macropinocytosis inhibition), 5 mmol/L methyl β-cyclodextrin (caveolin- and clathrin-independent inhibition; DMSO $\leq$ 0.5%v/v), and 1-hour co-incubation in complete growth medium supplanted with inhibitors and 0.1 nmol/L LbL nanoparticles (561 nm ex; 610/20 nm em). Immunofluorescence cytometry was performed using the FlowCellect Pathway Activation Kit (Millipore FCCS025100) and 100-nm fluorescent carboxylate-modified polystyrene beads (Life Technologies; Red 580/605) were used as surrogates for dextran sulfate–conjugated liposomes.

In vivo cytokine response

Hyaluronan- or dextran sulfate–LbL nanoparticles (8.3×10^{12} NP/kg, 5% glucose) were injected via the tail vein into 6- to 8-week-old female BALB/c mice ($n = 3$). Blood was withdrawn at 1 and 6 hours postinjection via retro-orbital bleed and 24 hours postinjection via cardiac puncture, into serum separator tubes (1,000 rcf, 4°C; Greiner Bio) and stored at −20°C until use. Serum was analyzed via magnetic bead–based multiplexed immunoassay (BioRad BioPlex 3D; 8-Plex Cytokine Panel) using a BIO-RAD Bio-Plex 3D Suspension Array System.

In vivo experiments

A total of 5×10^6 MDA-MB-231 cells (1:1 PBS:Matrigel) were injected subcutaneously into the hindflanks of nude mice (NCR *nu/nu*, Taconic). Tumors were allowed to form over 3 to 4 weeks, after which treatment groups were randomized. Nanoparticles (8.3×10^{12} NP/kg, 5% glucose) were injected via the tail vein into tumor-bearing nude or immunocompetent mice (BALB/c, Taconic). Whole-animal imaging was performed using a Xenogen IVIS Imaging System (Caliper) and 100-nm fluorescent carboxylate–modified polystyrene beads (Life Technologies; Infrared 715/755) as surrogates for dextran sulfate–conjugated liposomes. Free drugs were dosed o.g. at nanoparticle-equivalent drug concentrations (5% D-glucose, 1% polysorbate 80). Albumin, blood urea nitrogen (BUN), and creatinine (Cr) levels were measured by Charles River Laboratories from serum samples obtained via cardiac puncture 24 hours following nanoparticle (i.v.) or free drug (o.g.) administration in 6- to 8-week-old female BALC/c mice. These experiments were approved by the Massachusetts Institute of Technology Committee on Animal Care (CAC).

Histology

Hepatic lesion scores (48) were assigned as follows: grade 0, no evidence of histologic lesions; 1, minimal congestion and mild hepatocellular cytoplasmic degeneration immediately adjacent to the central vein; 2, moderate congestion and degeneration with individual necrotic hepatocytes in the periportal region; 3, marked congestion and degeneration with necrotic hepatocytes extending into the midzonal regions; 4, severe congestion and degeneration and necrosis that bridges between most centrilobular zones. Tissue samples were obtained at 24 hours following nanoparticle (i.v.) or free drug (o.g.) administration in 6- to 8-week-old female BALC/c or NCR nude mice for toxicologic or pharmacodynamics analysis, respectively. Tumors were lysed in RIPA buffer containing protease/phosphatase inhibitor and analyzed by Western blotting. Vital organs were formalin-fixed, paraffin-embedded, and processed by the Swanson Biotechnology Center (MIT).

Results

We selected AZD6244 (selumetinib), an allosteric inhibitor of Mek1/2, and PX-866, a wortmannin analogue and covalent inhibitor of PI3K, for their potent activity against MAPK oncogene–addicted solid tumors (33, 49, 50). Interestingly, AZD6244 (log*D* $\sim$ 5.55) and PX-866 (log*D* $\sim$ 2.26) exhibit vastly differing lipophilicities and would thus be challenging to entrap within a single polymer nanoparticle matrix such as poly(lactic acid-*co*-glycolic acid) (PLGA). Here, the 2 drugs were encapsulated by sonication/extrusion within cationic vesicles (90 $\pm$ 11 nm dia) composed of DOTAP with DOPE helper phospholipid (Fig. 1A and B). Polyelectrolyte multilayers were then self-assembled onto the drug-containing vesicle cores by alternating adsorption and centrifugation (24). The strongly ionized polyelectrolyte, dextran sulfate, was used to initially stabilize the carriers and impart anionic charge. Next, a hypoxic tumor pH-responsive and CD44 receptor–targeting bilayer of poly-(L-lysine) and hyaluronic acid were assembled onto the nanoparticles. Previously (24), we found that this architecture was capable of actively targeting the cancer stem cell marker, CD44, through hyaluronan binding and also selectively underwent a transition in surface charge and swelling at pH values <7, leading to both size-dependent passive

Published OnlineFirst June 1, 2015; DOI: 10.1158/1078-0432.CCR-15-0013

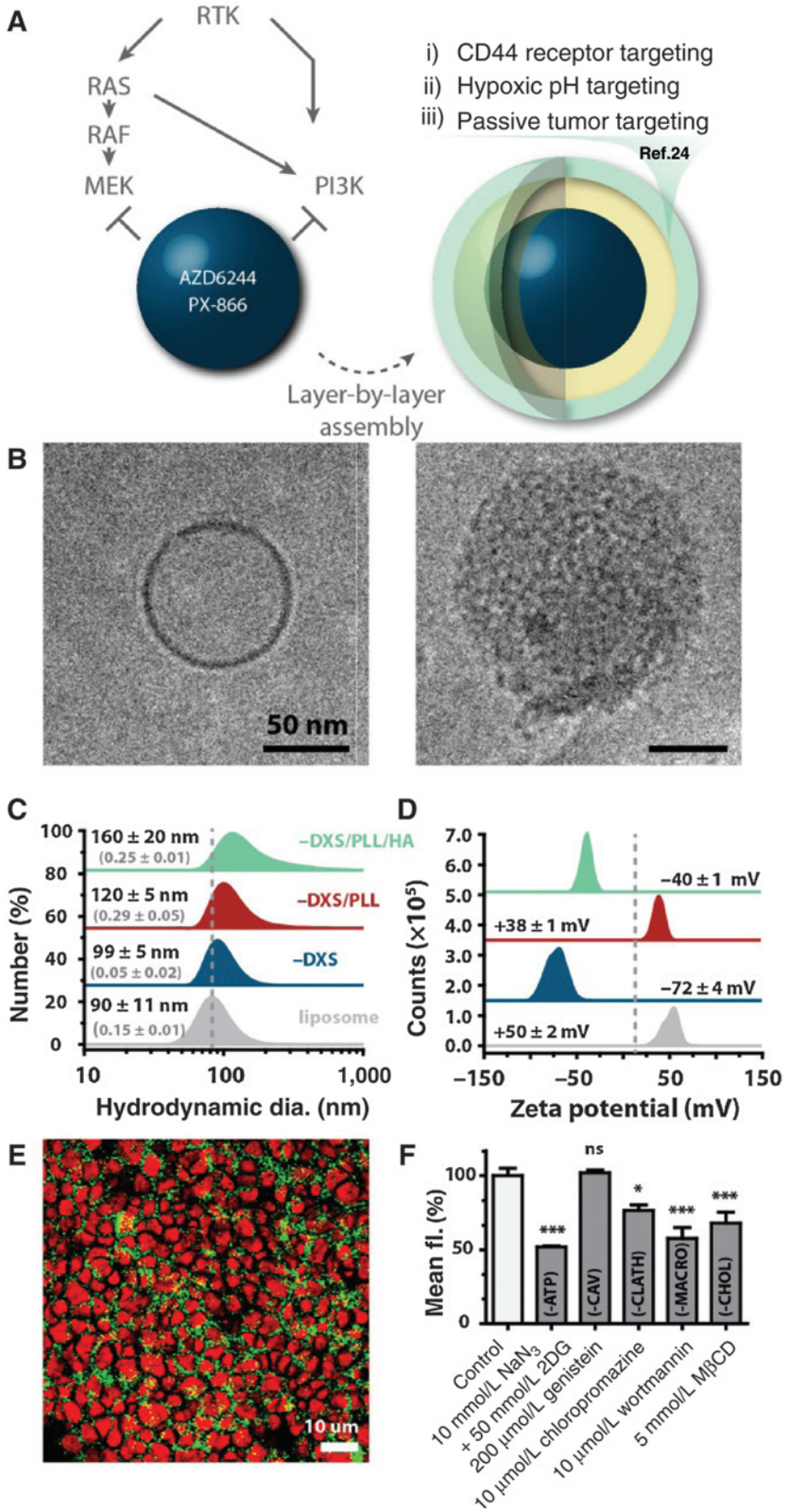

Figure 1.
An engineered LbL nanoparticle for tumor-targeted horizontal blockade of MAPK and PI3K signaling. A, schematic illustrating combined blockade of MEK (AZD6244) and PI3K (PX-866) via multimodal tumor-targeting LbL nanoparticles. B, cryogenic transmission electron microscopy (cryo-TEM) of cationic, drug-encapsulating liposomal cores (left) and tumor-targeting, LbL-coated liposomes (right). Size evolution (C) and corresponding surface charge shift (D) during the LbL assembly process as measured by dynamic light scattering and laser Doppler electrophoresis (zeta potential analysis), respectively. E, *in vitro* delivery and penetration of tumor-targeting LbL nanoparticles (green) into Hep G2 tumor spheroids (actin, red) as measured by confocal fluorescence microscopy. F, mechanistic analysis of LbL nanoparticle cell uptake (1 hour) as measured by flow cytometry of particle-treated MDA-MB-231 cell monolayers pretreated with inhibitors of various endocytotic pathways indicated. Polydispersity index (PDI) in (C) is reported in parentheses. Error represents (C and D) SD of 3 technical and (F) SEM of 3 biological replicates. *, $P < 0.05$; **, $P < 0.01$; ***, $P < 0.001$.

Published OnlineFirst June 1, 2015; DOI: 10.1158/1078-0432.CCR-15-0013

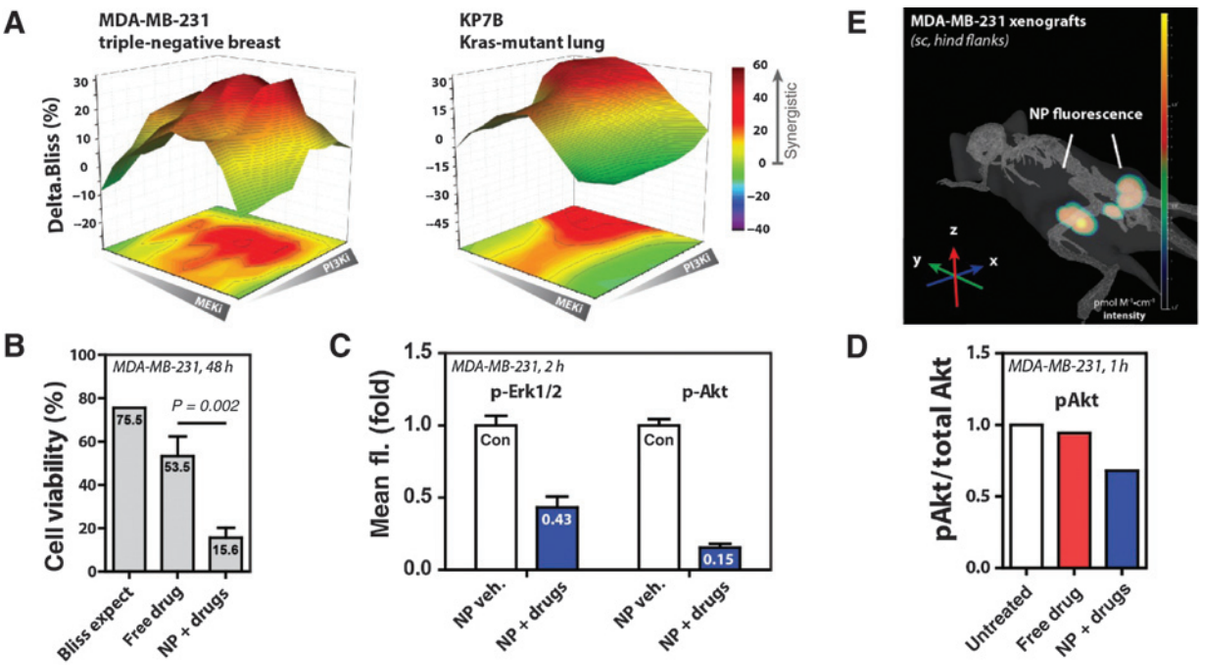

Figure 2.

Rational drug combination nanomedicines against MAPK/PI3K signaling synergistically kill tumor cell lines *in vitro* and target solid tumors *in vivo*. A, drug interaction matrix plotting cell killing observed in excess of the additive Bliss expectation between MEK and PI3K inhibition in triple-negative breast and RAS-mutant non–small cell lung carcinoma (MDA-MB-231, KP7B; 0.05–50 μmol/L, 48 hours). B, LbL nanoparticle encapsulation augments drug synergy *in vitro* and (C) horizontally blocks MAPK and PI3K signaling as measured by phospho-Erk1/2 and phospho-Akt cell staining, respectively. D, at early time points (10-minute serum stimulation), LbL nanoparticle–encapsulated drugs deplete relative pAkt more completely than the equivalent free drug combination. E, *in vivo* 3D fluorescence tomography of LbL nanoparticles indicates high colocalization with subcutaneous MDA-MB-231 tumor xenografts following systemic administration. B, 1.1 μmol/L AZD6244 and 3.5 μmol/L PX-866, 48 hours. C, 50 nmol/L AZD6244, 160 nmol/L PX-866, 2 hours, PBS; serum stimulation, 1 hour. D, 0.3 μmol/L AZD6244, 1 μmol/L PX-866, 1 hour; serum stimulation, 10 minutes. E, obtained with structured illumination of the lower abdomen (24 hours; 8.3×10^{12} NP/kg, 5% glucose; 715/760 ex/em). Error bars represent (B) SD of 4 technical and (C) SEM of 3 biological replicates.

tumor targeting and active targeting through both ligand-directed and hypoxic pH–responsive delivery.

Layer-by-layer assembly onto the drug-loaded particle cores yielded 160 ± 20 nm dia nanoparticle drug carriers as the final product (Fig. 1B and C; 2.7 wt% AZD6244, 10 wt% PX-866). Hydrodynamic size evolution during the LbL self-assembly process was monitored by cryogenic-transmission electron microscopy (cryo-TEM, Fig. 1B), dynamic light scattering (Fig. 1C), and laser Doppler electrophoresis (Fig. 1D), indicating size increase and corresponding charge shift with each successive layer. In addition to its tumor targeting capabilities (24), the LbL architecture was also used to decrease nonspecific drug leakage from the particles (51). *In vitro*, fluorescent LbL nanoparticles penetrated 3-dimensional (3D) tumor spheroids with high efficiency (Fig. 1E), likely a result of the highly hydrated, anionic, and protein-repellent outer hyaluronan shell (24). The particles also exhibited cell uptake through ATP-dependent mechanisms including clathrin-mediated, macropinocytotic, and cholesterol-mediated processes (Fig. 1F) as assessed by flow cytometry. In agreement with previous reports investigating cellular interactions with hyaluronan-conjugated nanoparticles, we found that LbL nanoparticle uptake here was partially mediated by interactions with lipid rafts (52), as indicated by a 32% loss in uptake following cholesterol depletion using methyl-β-cyclodextrin. We also observe contributions from clathrin-mediated and micropinocytosis processes which have also been implicated in the cellular uptake of free hyaluronan (53).

We additionally investigated combinatorial interactions between Mek and PI3K blockade using free drugs *in vitro*, as measured by the amount of (synergistic) cell killing in excess of the additive Bliss expectation (47; 48 hours, see Materials and Methods for details). Horizontal blockade was synergistic in triple-negative breast (MDA-MB-231) and murine-derived Ras-mutant non–small cell lung carcinoma (Fig. 2A), but interestingly, not in an epithelial ovarian cancer cell line (OVCAR3; Supplementary Fig. S1), in agreement with that cell line's lack of MAPK/PI3K mutations that predicate response (e.g., activating mutations in *Ras*, *BRAF*, or *PI3K*; loss of *PTEN*; ref. 54). These results are also in agreement with Hoeflich and colleagues (55) and Iadevaia and colleagues (56) who predicted synergistic cell killing of basal-like (triple-negative) breast carcinoma following dual blockade of MAPK and PI3K. Likewise, Engelman and colleagues (33) demonstrated that combined pathway signaling is required for Ras-dependent tumor initiation, whereas Downward and colleagues found that dual pathway activation is required for Ras-dependent tumor maintenance (42) and angiogenesis (43). Interestingly, LbL nanoparticle encapsulation *further* improved synergistic cell killing in MDA-MB-231 cells by 2.6-fold, consistent with simultaneous blockade of pErk1/2 and pAkt staining as measured by immunofluorescence cytometry

Published OnlineFirst June 1, 2015; DOI: 10.1158/1078-0432.CCR-15-0013

(Fig. 2B and C). While studies are currently under way to elucidate the precise mechanism of nanoparticle-enhanced drug synergy, the results here may result from nanoparticle-accelerated or -augmented intracellular transport or simultaneous intracellular delivery of the hydrophobic–hydrophilic drug pair. Delivery of the 2 drugs, directly, may also lead to differential cell uptake for the drug pair that have notably disparate physiochemical properties. Kinetics of uptake and release may also be a factor. Interestingly, we found that at early time points (10-minute serum stimulation following 1 hour of drug treatment), nanoparticle inhibition of pAkt was more complete than from equivalent concentrations of the free drug combination (Fig. 2D), potentially abrogating PI3K pathway-mediated apoptotic suppression, at minimum (57). Using an *in vivo* mouse model, LbL nanoparticles targeted subcutaneous, CD44-expressing, triple-negative breast (MDA-MB-231) carcinoma tumors with high efficiency (Fig. 2E), suggesting that Mek and PI3K inhibitor–loaded LbL nanoparticles may be effective in treating solid tumors *in vivo*.

We next investigated LbL nanoparticle–mediated horizontal blockade in mice bearing subcutaneous MDA-MB-231 tumor xenografts. Western blot analyses from excised tumor lysates indicated a significant reduction in downstream signaling of both pathways 24 hours following intravenous administration of the targeted nanoparticles (1 mg/kg AZD6244, 3.7 mg/kg PX-866, Fig. 3A). Phosphorylation of Erk1/2 and Akt were reduced 3.9- and 9.4-fold, respectively, following nanoparticle delivery

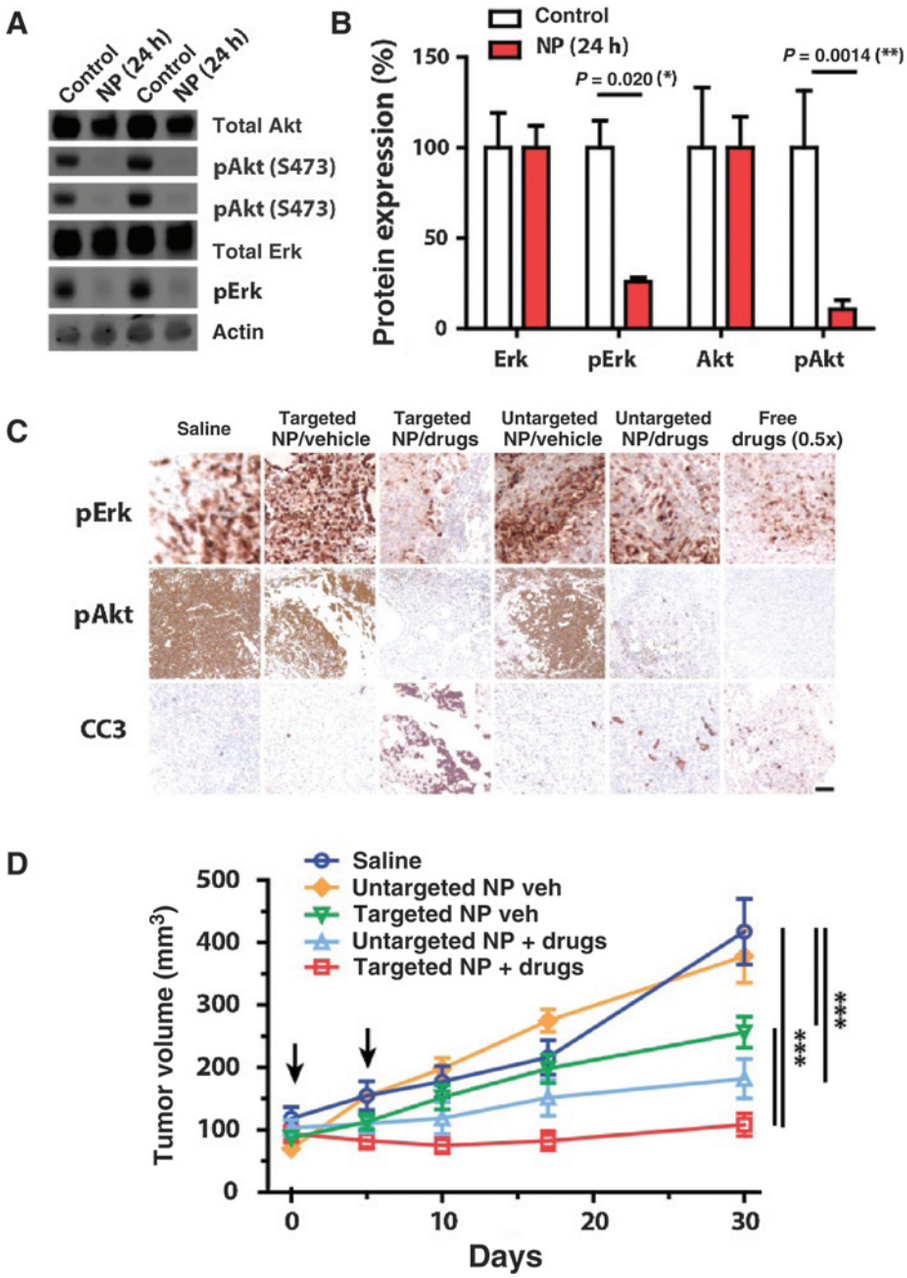

Figure 3.
Tumor-targeting LbL nanoparticles horizontally block tumor-specific MAPK/PI3K signaling and induce disease stabilization *in vivo*. A, combined signal blockade as measured by decreased phosphorylation of Akt and Erk1/2 as measured by Western blotting and (B) densitometry from tumor lysates of untreated and nanoparticle-treated mice bearing subcutaneous MDA-MB-231 xenografts 24 hours following i.v. administration of LbL nanoparticles. C, histologic analysis of corresponding tumor sections indicating decreased phospho-Erk1/2 and phospho-Akt staining, as well as increased cell death as measured by cleaved caspase-3 (CC3). D, *in vivo* treatment response following i.v. nanoparticle administration on days 0 and 5 ($n = 5$). Lanes 3 and 4 are technical replicates of lanes 1 and 2 in A. Scale bar in (C) is 200 μm. Error bars represent (B) SD of 2 to 4 technical and (D) SEM of 5 biological replicates. *, $P < 0.05$; **, $P < 0.01$; ***, $P < 0.001$.

Published OnlineFirst June 1, 2015; DOI: 10.1158/1078-0432.CCR-15-0013

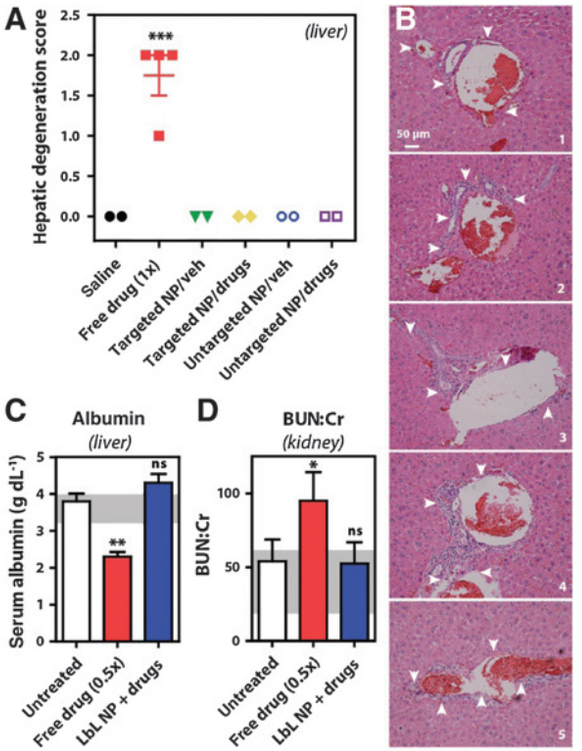

Figure 4.

LbL nanoparticles improve the therapeutic index of dual MAPK/PI3K pathway inhibition. A, hepatic degeneration score as assessed from hematoxylin and eosin (H&E)-stained liver sections from immunocompetent BALB/c mice 24 hours following combination drug administration as targeted and untargeted LbL nanoparticle formulations, as well as their respective vehicles, in comparison to a lethal equivalent dose of the free drug combination. B, H&E-stained liver sections from MDA-MB-231 tumor xenograft-bearing NCR nude mice ($n = 5$) 24 hours following administration of free AZD6244 and free PX-866 (1 mg/kg AZD6244, 3.7 mg/kg PX-866 o.g.). Arrowheads indicate damage to tissues surrounding the hepatic central vein and bile ducts including fragmented nuclei and extravasated erythrocytes. C and D, nanoparticle-rescued hepatic and renal function as measured from serum albumin, BUN, and creatinine levels 24 hours following combination drug administration as an LbL nanoparticle formulation and as a sublethal (0.5×) free drug combination in immunocompetent BALB/c mice. Shaded area in C and D denotes normal murine reference ranges (95% CI) from ref. 60. Error represents SEM of 2 to 5 biological replicates. *, $P < 0.05$; **, $P < 0.01$; ***, $P < 0.001$.

(Fig. 3B). These effects were corroborated by immunohistochemical staining, which also correlated with an increase in apoptotic tumor cell killing as indicated by increased staining of cleaved caspase-3 (Fig. 3C).

We further investigated effects from LbL nanoparticle tumor targeting on subsequent treatment outcomes from horizontal blockade. Mice treated with tumor-targeted LbL nanoparticles exhibited significant disease stabilization (16% ± 11% at day 30) following intravenous administration of dual drug–containing particles (Fig. 3D). In contrast, mice similarly treated with nontargeting control LbL nanoparticles of comparable size and charge (Fig. 3D, "untargeted") exhibited slowed, but progressive disease (80% ± 50% at day 30). Interestingly, tumor-targeted vehicle LbL nanoparticles that did not contain drug elicited a small but significant (1.6 ± 0.8-fold) decrease in tumor size relative to untreated controls, a response which may be attributable to antiproliferative interactions between high molecular mass hyaluronan (58) on the LbL particle surface and CD44 receptors expressed highly on triple-negative breast cell lines including MDA-MB-231 (24). Equivalent doses of the free drugs were poorly tolerated, resulting in rapid morbidity and mortality in tumor-bearing mice. Histologic analysis of tissue sections from vital organs (24 hours) indicated significant damage in tissues surrounding the hepatic central vein and bile ducts (Fig. 4A and B), including fragmented nuclei and erythrocyte extravasation following administration of the free drug combination. In contrast, mice that received drug-containing LbL nanoparticles—both targeted and untargeted—exhibited no significant histopathologic differences with controls or vehicles alone. Interestingly, immunocompetent mice receiving a half-equivalent dose of the free drug combination exhibited a significant decrease in serum albumin (1.5 ± 0.3 g/dL) and a 40 ± 20-fold elevation in serum blood urea nitrogen:creatinine (BUN:Cr) levels (Fig. 4C and D), indicative of impaired hepatic and renal function, respectively, whereas mice receiving a full dose of the tumor-targeted LbL nanoparticle formulation exhibited no significant changes in serum albumin, BUN, or Cr. Collectively, these data indicate that LbL nanoparticle encapsulation can direct tissue disposition of drug combinations in a manner that enhances their therapeutic index—in addition to drug synergy. Biochemical and histopathologic damage observed here from the free drug combination is consistent with a previous phase I clinical trial investigating horizontal blockade in patients with refractory solid tumors that reported dose-limiting hepatic toxicity as a common grade >3 adverse event (45), consistent with the hepatic damage we observed in this murine model. Interestingly, mice receiving tumor-targeted LbL nanoparticles exhibited no significant change in body condition and only transient changes in serum cytokine levels (Supplementary Fig. S2). These findings may be attributable to improved tissue distribution profiles of these novel drug carriers, where we previously observed 4-fold improved tumor targeting (ca. 6%ID) and 2-fold decreased liver accumulation in tumor-bearing and immunocompetent mice, respectively, compared with nontargeting LbL nanoparticle architectures (24). Together, these findings suggest that LbL nanoparticle–mediated horizontal blockade could be impactful in improving treatment outcomes in solid tumors driven by MAPK or PI3K axis signaling.

Discussion

Simultaneous blockade of MAPK and PI3K pathway signaling has been shown to synergistically kill a variety of solid tumors *in vivo* and abrogate resistance-associated signaling (33, 42, 44, 55). Shimizu and colleagues, in a retrospective phase I clinical study of 236 patients with advanced solid tumors receiving small-molecule MAPK or PI3K pathway inhibitors, alone or in combination, found that combined blockade elicited favorable treatment response in the advanced disease population. This favorable response, however, came at the expense of greater toxicity, resulting in a 2.0-fold increased prevalence of dose-limiting toxicity and a 3.0-fold increased prevalence of drug-related grade >3 adverse events (45). Nanoscale drug formulations such as Abraxane and Doxil can enhance therapeutic index in patients (5) and improve treatments outcomes in combination delivery approaches (6, 9, 12, 14). Previously, we demonstrated that an emerging class of nanoscale drug carrier, LbL nanoparticles, could improve

Published OnlineFirst June 1, 2015; DOI: 10.1158/1078-0432.CCR-15-0013

tumor accumulation 4.0-fold and decrease liver accumulation 2.0-fold (24). We hypothesized that the enhanced tissue disposition profiles afforded by these novel drug carriers could improve tumor cell killing from dual MAPK/PI3K inhibition while reducing drug-related hepatotoxicity such as that indicated by increased transaminase levels reported by Shimizu and colleagues. An improved safety profile could potentially augment tolerable dosing levels in patients and further improve response rates to dual MAPK/PI3K pathway inhibition in the clinic.

LbL nanoparticles containing AZD6244 (selumetinib), an allosteric inhibitor of Mek1/2, and PX-866, a covalent inhibitor of PI3K, were 160 ± 20 nm in hydrodynamic diameter, well below the size-dependent splenic clearance threshold, and negative in surface charge (-40 ± 1 mV) to prevent nonspecific cell surface interactions. In previous studies, we found that these architectures could circulate for long periods following i.v. bolus injection (elimination half-life $\sim$ 28 hours; ref. 8) target tumors with high efficiency and decrease liver-specific accumulation (24). *In vitro*, these nanoscale formulations entered cells through various ATP-dependent processes (excluding caveolin-dependent entry), simultaneously blocked MAPK and PI3K pathway activation, and exhibited synergistic cell killing in excess of the additive Bliss expectation. Interestingly, we found that drug synergy was further enhanced following nanoscale encapsulation, a factor that could also further improve the therapeutic index of dual MAPK/PI3K blockade in the clinic. Consistent with patient responders in Shimizu and colleagues harboring co-activation of both MAPK and PI3K pathway signaling, we observed synergistic cell killing in basal-like MDA-MB-231 breast cells which harbor an activating mutation in *KRAS* (G12V), high levels of EGFR protein, and *PTEN*-dependent survival following MEK inhibition (55). We further observed drug synergy in KP7B cells derived from an autochthonous mouse model of non–small cell lung cancer which host an activating mutation in *KRAS* (G12D) but not in OVCAR3 epithelial ovarian cancer cells, which lack any predicating mutations on either axis (*PI3KCA*, *PTEN*, *KRAS*, and *BRAF*).

As a proof-of-concept, we investigated tumor remediation *in vivo* using a subcutaneous MDA-MB-231 xenograft mouse model. Following a single i.v. bolus injection, we observed significant disease stabilization from our tumor-targeting nanoscale drug formulation but progressive disease in our nontargeting control. This response was accompanied by a reduction in tumor-specific phosphorylation of the terminal kinases Erk and Akt and an increase in apoptosis as histologically measured by cleaved caspase-3 staining. Interestingly, combination therapy with the free drugs was lethal at equivalent dosing and, at sublethal dosing levels, resulted in acute hepatic and renal dysfunction as measured by decreased serum albumin and elevated BUN:Cr levels, as well as gross histopathologic liver damage at the full equivalent dose. These findings are consistent with dose-limiting hepatic toxicity reported in phase I trial patients receiving dual MAPK/PI3K blockade therapy (45). These nanoscale formulations were well-tolerated in tumor-bearing mice and elicited in no acute serum cytokine upregulation following systemic administration in immunocompetent mice, as well as no significant changes in hepatic or renal function as measured from serum blood chemistry and histopathologic analysis of vital organs. Studies are currently under way to identify and profile surviving cell subpopulations, optimize dosing regimens, and investigate therapeutic response in advanced tumor models. While murine xenografts exhibit notable functional and pathologic differences with human breast carcinomas (e.g., stromal compaction, labeling index, and vascularity) these results are particularly promising in the context of prior work investigating related LbL nanoparticle architectures that demonstrate the ability to target and treat tumors in other sites including orthotopic mammary fat pad (59) and autochthonous lung tumor models (unpublished data). Although here we found these particles capable of rapid diffusion throughout tumor spheroid models, efficient intratumoral distribution and the capacity to target poorly vascularlized tumors remains a key challenge for these and other emerging classes of nanoscale drug carriers. Efforts to further engineer modular LbL nanoparticle delivery platforms that improve therapeutic safety, potency, and durability are currently under way.

In summary, here we developed a tumor-targeting nanoscale drug formulation based on LbL self-assembly that horizontally blocks MAPK and PI3K signaling *in vitro* and *in vivo*, selectively inhibiting disease progression in tumor-bearing mice. These self-assembled drug carriers co-delivered small-molecule inhibitors of MEK and PI3K with vastly differing physiochemical properties and enhanced synergistic cell killing 2.6-fold following encapsulation. Following systemic administration in breast tumor xenograft–bearing mice, we observed a 3.9- and 9.4-fold reduction in tumor-specific MAPK and PI3K pathway signaling, respectively, accompanied by tumor apoptosis and disease stabilization in the absence of dose-limiting hepatotoxic effects observed from the free drug combination. Mice receiving untargeted, but dual drug–loaded nanoscale formulations, exhibited progressive disease. Tumor-targeting nanoscale drug formulations could provide a more safe and effective means to synergistically block MAPK and PI3K in the clinic.

Disclosure of Potential Conflicts of Interest

R. Drapkin is a consultant/advisory board member for Siamab Therapeutics. No potential conflicts of interest were disclosed by the other authors.

Authors' Contributions

Conception and design: E.C. Dreaden, S.W. Morton, K.Y. Choi, K. Renggli, M.B. Yaffe, P.T. Hammond
Development of methodology: E.C. Dreaden, K.Y. Choi, P.T. Hammond
Acquisition of data (provided animals, acquired and managed patients, provided facilities, etc.): E.C. Dreaden, Y.W. Kong, S.W. Morton, S. Correa, K.Y. Choi, K.E. Shopsowitz, K. Renggli, R. Drapkin
Analysis and interpretation of data (e.g., statistical analysis, biostatistics, computational analysis): E.C. Dreaden, Y.W. Kong, S.W. Morton, K.Y. Choi, K.E. Shopsowitz, K. Renggli, R. Drapkin, M.B. Yaffe, P.T. Hammond
Writing, review, and/or revision of the manuscript: E.C. Dreaden, Y.W. Kong, S.W. Morton, S. Correa, K.E. Shopsowitz, R. Drapkin, M.B. Yaffe, P.T. Hammond
Administrative, technical, or material support (i.e., reporting or organizing data, constructing databases): E.C. Dreaden
Study supervision: M.B. Yaffe, P.T. Hammond

Acknowledgments

The authors thank the Koch Institute Swanson Biotechnology Center for technical support, specifically the FACS, Peterson nanotechnology, microscopy, ATWAI, and Tang Histology facilities. They also thank Roderick T. Bronson and Marianna Sofman for assistance with histologic analyses, as well as Mohi Quadir, Brian S. Aitken, Young Hoon Roh, Julio D'Arcy, Kathy Cormier, Dong Soo Yun, and Eliza Vasile for helpful discussions.

Grant Support

This work was supported by the Breast Cancer Alliance (M.B. Yaffe, P.T. Hammond; Exceptional Project), the Department of Defense (P.T. Hammond; OCRP Teal Innovator Award), the NIH (E.C. Dreaden; NIBIB 1F32EB017614-02), the Dr. Miriam and Sheldon G. Adelson Medical Research Foundation

(R. Drapkin), the Honorable Tina Brozman Foundation (R. Drapkin), the Misrock Foundation (Y.W. Kong), the US National Science Foundation (S.W. Morton), and the Swiss National Science Foundation (K. Renggli). Support was provided in part by the Koch Institute Support Grant (P30-CA14051) from the National Cancer Institute and the MIT MRSEC Shared Experimental Facilities Grant (DMR-0819762) from the National Science Foundation.

The costs of publication of this article were defrayed in part by the payment of page charges. This article must therefore be hereby marked *advertisement* in accordance with 18 U.S.C. Section 1734 solely to indicate this fact.

Received January 4, 2015; revised April 29, 2015; accepted May 12, 2015; published OnlineFirst June 1, 2015.

References

1. Moxley JH, De Vita VT, Brace K, Frei E. Intensive combination chemotherapy and X-irradiation in Hodgkin's disease. Cancer Res 1967;27:1258–63.
2. DeVita VJr, Simon R, Hubbard S, Young R, Berard C, Moxley J III, et al. Curability of advanced Hodgkin's disease with chemotherapy. Long-term follow-up of MOPP-treated patients at the National Cancer Institute. Ann Intern Med 1980;92:587–95.
3. Corcoran R, Cheng K, Hata A, Faber A, Ebi H, Coffee E, et al. Synthetic lethal interaction of combined BCL-XL and MEK inhibition promotes tumor regressions in KRAS mutant cancer models. Cancer Cell 2013;23:121–8.
4. Basu S, Harfouche R, Soni S, Chimote G, Mashelkar RA, Sengupta S. Nanoparticle-mediated targeting of MAPK signaling predisposes tumor to chemotherapy. Proc Nat Acad Sci U S A 2009;106:7957–61.
5. Sengupta S, Eavarone D, Capila I, Zhao G, Watson N, Kiziltepe T, et al. Temporal targeting of tumour cells and neovasculature with a nanoscale delivery system. Nature 2005;436:568–72.
6. Pandey A, Kulkarni A, Roy B, Goldman A, Sarangi S, Sengupta P, et al. Sequential application of a cytotoxic nanoparticle and a PI3K inhibitor enhances antitumor efficacy. Cancer Res 2014;74:675–85.
7. Hegde G, de la Cruz C, Chiu C, Alag N, Schaefer G, Crocker L, et al. Blocking NRG1 and other ligand-mediated Her4 signaling enhances the magnitude and duration of the chemotherapeutic response of non-small cell lung cancer. Sci Transl Med 2013;5:171ra18.
8. Deng ZJ, Morton SW, Ben-Akiva E, Dreaden EC, Shopsowitz KE, Hammond PT. Layer-by-layer nanoparticles for systemic codelivery of an anticancer drug and siRNA for potential triple-negative breast cancer treatment. ACS Nano 2013;7:9571–84.
9. Blanco E, Sangai T, Wu S, Hsiao A, Ruiz-Esparza GU, Gonzalez-Delgado CA, et al. Colocalized delivery of rapamycin and paclitaxel to tumors enhances synergistic targeting of the PI3K/Akt/mTOR Pathway. Mol Ther 2014;22:1310–9.
10. Johnson N, Li Y-CC, Walton ZE, Cheng KA, Li D, Rodig SJ, et al. Compromised CDK1 activity sensitizes BRCA-proficient cancers to PARP inhibition. Nat Med 2011;17:875–82.
11. Lee Michael J, Ye Albert S, Gardino Alexandra K, Heijink Anne M, Sorger Peter K, MacBeath G, et al. Sequential application of anticancer drugs enhances cell death by rewiring apoptotic signaling networks. Cell 2012;149:780–94.
12. Morton SW, Lee MJ, Deng ZJ, Dreaden EC, Siouve E, Shopsowitz KE, et al. A nanoparticle-based combination chemotherapy delivery system for enhanced tumor killing by dynamic rewiring of signaling pathways. Sci Signal 2014;7:ra44.
13. Frei E. Curative cancer chemotherapy. Cancer Res 1985;45:6523–37.
14. Ma L, Kohli M, Smith A. Nanoparticles for combination drug therapy. ACS Nano 2013;7:9518–25.
15. Caruso F, Caruso RA, Mohwald H. Nanoengineering of inorganic and hybrid hollow spheres by colloidal templating. Science 1998;282:1111–4.
16. Donath E, Sukhorukov GB, Caruso F, Davis SA, Möhwald H. Novel hollow polymer shells by colloid templated assembly of polyelectrolytes. Angew Chem Int Ed 1998;37:2201–5.
17. Shutava TG, Balkundi SS, Vangala P, Steffan JJ, Bigelow RL, Cardelli JA, et al. Layer-by-layer-coated gelatin nanoparticles as a vehicle for delivery of natural polyphenols. ACS Nano 2009;3:1877–85.
18. Schneider G, Decher G. From functional core/shell nanoparticles prepared via layer-by-layer deposition to empty nanospheres. Nano Lett 2004;4:1833–9.
19. Zahr A, de Villiers M, Pishko M. Encapsulation of drug nanoparticles in self-assembled macromolecular nanoshells. Langmuir 2005;21:403–10.
20. Agarwal A, Lvov Y, Sawant R, Torchilin V. Stable nanocolloids of poorly soluble drugs with high drug content prepared using the combination of sonication and layer-by-layer technology. J Controll Release 2008;128:255–60.
21. Poon Z, Chang D, Zhao X, Hammond PT. Layer-by-Layer Nanoparticles with a pH-Sheddable layer for *in vivo* targeting of tumor hypoxia. ACS Nano 2011;5:4284–92.
22. Poon Z, Lee JB, Morton SW, Hammond PT. Controlling *in vivo* stability and biodistribution in electrostatically assembled nanoparticles for systemic delivery. Nano Lett 2011;11:2096–103.
23. Hammond PT. Polyelectrolyte multilayered nanoparticles: using nanolayers for controlled and targeted systemic release. Nanomedicine 2012;7:619–22.
24. Dreaden EC, Morton SW, Shopsowitz KE, Choi J-H, Deng ZJ, Cho N-J, et al. Bimodal tumor-targeting from microenvironment responsive hyaluronan layer-by-Layer (LbL) nanoparticles. ACS Nano 2014;8:8374–82.
25. Sebolt-Leopold J, Herrera R. Targeting the mitogen-activated protein kinase cascade to treat cancer. Nat Rev Cancer 2004;4:937–47.
26. Vivanco I, Sawyers C. The phosphatidylinositol 3-Kinase AKT pathway in human cancer. Nat Rev Cancer 2002;2:489–501.
27. Johnson L, Mercer K, Greenbaum D, Bronson R, Crowley D, Tuveson D, et al. Somatic activation of the K-ras oncogene causes early onset lung cancer in mice. Nature 2001;410:1111–6.
28. Shaw AT, Winslow MM, Magendantz M, Ouyang C, Dowdle J, Subramanian A, et al. Selective killing of K-ras mutant cancer cells by small molecule inducers of oxidative stress. Proc Natl Acad Sci U S A 2011;108:8773–8.
29. Davies H, Bignell G, Cox C, Stephens P, Edkins S, Clegg S, et al. Mutations of the BRAF gene in human cancer. Nature 2002;417:949–54.
30. Salmena L, Carracedo A, Pandolfi P. Tenets of PTEN tumor suppression. Cell 2008;133:403–14.
31. Samuels Y, Wang Z, Bardelli A, Silliman N, Ptak J, Szabo S, et al. High frequency of mutations of the PIK3CA gene in human cancers. Science 2004;304:554.
32. Tuveson D, Shaw A, Willis N, Silver D, Jackson E, Chang S, et al. Endogenous oncogenic K-ras(G12D) stimulates proliferation and widespread neoplastic and developmental defects. Cancer Cell 2004;5:375–87.
33. Engelman JA, Chen L, Tan X, Crosby K, Guimaraes AR, Upadhyay R, et al. Effective use of PI3K and MEK inhibitors to treat mutant Kras G12D and PIK3CA H1047R murine lung cancers. Nat Med 2008;14:1351–6.
34. Janku F, Lee J, Tsimberidou A, Hong D, Naing A, Falchook G, et al. PIK3CA mutations frequently coexist with RAS and BRAF mutations in patients with advanced cancers. PLoS ONE 2011;6:e22769.
35. Carracedo A, Pandolfi P. The PTEN-PI3K pathway: of feedbacks and cross-talks. Oncogene 2008;27:5527–41.
36. Serra V, Scaltriti M, Prudkin L, Eichhorn P, Ibrahim Y, Chandarlapaty S, et al. PI3K inhibition results in enhanced HER signaling and acquired ERK dependency in HER2-overexpressing breast cancer. Oncogene 2011;30:2547–57.
37. Cen B, Mahajan S, Wang W, Kraft A. Elevation of receptor tyrosine kinases by small molecule AKT inhibitors in prostate cancer is mediated by Pim-1. Cancer Res 2013;73:3402–11.
38. Carracedo A, Ma L, Teruya-Feldstein J, Rojo F, Salmena L, Alimonti A, et al. Inhibition of mTORC1 leads to MAPK pathway activation through a PI3K-dependent feedback loop in human cancer. J Clin Invest 2008;118:3065–74.
39. Engelman JA, Zejnullahu K, Mitsudomi T, Song Y, Hyland C, Park JO, et al. MET amplification leads to gefitinib resistance in lung cancer by activating ERBB3 signaling. Science 2007;316:1039–43.
40. Straussman R, Morikawa T, Shee K, Barzily-Rokni M, Qian Z, Du J, et al. Tumour micro-environment elicits innate resistance to RAF inhibitors through HGF secretion. Nature 2012;487:500–4.
41. Wee S, Jagani Z, Xiang KX, Loo A, Dorsch M, Yao Y-M, et al. PI3K pathway activation mediates resistance to MEK inhibitors in KRAS mutant cancers. Cancer Res 2009;69:4286–93.

42. Castellano E, Sheridan C, Thin M, Nye E, Spencer-Dene B, Diefenbacher M, et al. Requirement for interaction of PI3-Kinase p110α with RAS in lung tumor maintenance. Cancer Cell 2013;24:617–30.
43. Murillo MM, Zelenay S, Nye E, Castellano E, Lassailly F, Stamp G, et al. RAS interaction with PI3K p110α is required for tumor-induced angiogenesis. J Clin Invest 2014;124:3601–11.
44. Posch C, Moslehi H, Feeney L, Green G, Ebaee A, Feichtenschlager V, et al. Combined targeting of MEK and PI3K/mTOR effector pathways is necessary to effectively inhibit NRAS mutant melanoma *in vitro* and *in vivo*. Proc Natl Acad Sci U S A 2013;110:4015–20.
45. Shimizu T, Tolcher AW, Papadopoulos KP, Beeram M, Rasco DW, Smith LS, et al. The clinical effect of the dual-targeting strategy involving PI3K/AKT/mTOR and RAS/MEK/ERK pathways in patients with advanced cancer. Clin Cancer Res 2012;18:2316–25.
46. DuPage M, Dooley AL, Jacks T. Conditional mouse lung cancer models using adenoviral or lentiviral delivery of Cre recombinase. Nat Prot 2009;4:1064–72.
47. Borisy AA, Elliott PJ, Hurst NW, Lee MS, Lehár J, Price ER, et al. Systematic discovery of multicomponent therapeutics. Proc Natl Acad Sci U S A 2003;100:7977–82.
48. Wancket LM, Meng X, Rogers LK, Liu Y. Mitogen-activated protein kinase phosphatase (Mkp)-1 protects mice against acetaminophen-induced hepatic injury. Toxicol Pathol 2012;40:1095–105.
49. Chen Z, Cheng K, Walton Z, Wang Y, Ebi H, Shimamura T, et al. A murine lung cancer co-clinical trial identifies genetic modifiers of therapeutic response. Nature 2012;483:613–20.
50. Yang Y, Iwanaga K, Raso MG, Wislez M, Hanna AE, Wieder ED, et al. Phosphatidylinositol 3-Kinase mediates bronchioalveolar stem cell expansion in mouse models of oncogenic *K-ras*-Induced lung cancer. PLoS ONE 2008;3:e2220.
51. Morton S, Poon Z, Hammond P. The architecture and biological performance of drug-loaded LbL nanoparticles. Biomaterials 2013;34:5328–35.
52. Qhattal HSS, Liu X. Characterization of CD44-Mediated cancer cell uptake and intracellular distribution of hyaluronan-grafted liposomes. Mol Pharm 2011;8:1233–46.
53. Greyner HJ, Wiraszka T, Zhang L-S, Petroll WM, Mummert ME. Inducible macropinocytosis of hyaluronan in B16-F10 melanoma cells. Matrix Biol 2010;29:503–10.
54. Domcke S, Sinha R, Levine DA, Sander C, Schultz N. Evaluating cell lines as tumour models by comparison of genomic profiles. Nat Comm 2013;4:2126.
55. Hoeflich K, O'Brien C, Boyd Z, Cavet G, Guerrero S, Jung K, et al. *In vivo* antitumor activity of MEK and phosphatidylinositol 3-kinase inhibitors in basal-like breast cancer models. Clin Cancer Res 2009;15:4649–64.
56. Iadevaia S, Lu YL, Morales FC, Mills GB, Ram PT. Identification of optimal drug combinations targeting cellular networks: integrating phosphoproteomics and computational network analysis. Cancer Res 2010;70:6704–14.
57. Mirzoeva OK, Das D, Heiser LM, Bhattacharya S, Siwak D, Gendelman R, et al. Basal subtype and MAPK/ERK Kinase (MEK)-Phosphoinositide 3-Kinase feedback signaling determine susceptibility of breast cancer cells to MEK inhibition. Cancer Res 2009;69:565–72.
58. Tian X, Azpurua J, Hine C, Vaidya A, Myakishev-Rempel M, Ablaeva J, et al. High-molecular-mass hyaluronan mediates the cancer resistance of the naked mole rat. Nature 2013;499:346–9.
59. Ngamcherdtrakul W, Morry J, Gu S, Castro DJ, Goodyear SM, Sangvanich T, et al. Cationic polymer modified mesoporous silica nanoparticles for targeted siRNA delivery to HER2+ breast cancer. Adv Funct Mater 2015;25:2646–59.
60. Schnell MA, Hardy C, Hawley M, Propert KJ, Wilson JM. Effect of blood collection technique in mice on clinical pathology parameters. Hum Gene Ther 2002;13:155–61.

Published OnlineFirst June 1, 2015; DOI: 10.1158/1078-0432.CCR-15-0013

Clinical Cancer Research

Tumor-Targeted Synergistic Blockade of MAPK and PI3K from a Layer-by-Layer Nanoparticle

Erik C. Dreaden, Yi Wen Kong, Stephen W. Morton, et al.

Clin Cancer Res 2015;21:4410-4419. Published OnlineFirst June 1, 2015.